ISSN 1512-1461

UDC: 538.9 Condensed matter Physics, Solid state Physics, Theoretical Condensed matter Physics

# VACUUM-EVAPORATED KESTERITE (CZTSSe) FOR SOLAR CELL APPLICATIONS

Zhengqi Shi and Ahalapitiya H. Jayatissa*

Department of Mechanical, Industrial, and Manufacturing Engineering, University of Toledo, OH 43606, USA
*Corresponding Author: ajayati@utnet.utoledo.edu

**Abstract**

*Kesterite $Cu_2ZnSn(S,Se)_4$ (CZTSSe) powder is synthesized by an aqueous hydrothermal process. Thin films of CZTSSe powder is fabricated by a vacuum thermal evaporation method and a mild sulfurization treatment. The vacuum coated CZTSSe film has mixed wurtzite and kesterite structure as identified by X-ray diffraction and no secondary phase is determined in the Raman spectroscopy. A high absorption coefficient at $10^4$ $cm^{-1}$ level and the bandgap of 1.53 eV are estimated from UV/visible spectrophotometry. Superstrate CZTSSe thin film solar cell is fabricated by using vacuum-evaporated CZTSSe films. The best solar cell shows an efficiency of 1.5% with a boosted short-circuit current density ($J_{sc}$) of 15.6 $mA/cm^2$, which is by far the highest efficiency for vacuum-based superstrate CZTSSe solar cells. Substrate-configured CZTSSe cells are also fabricated on Mo/SLG substrates and they show a slightly higher efficiency of 2.0% and 2.2% with and without the addition of ZnO between CdS and front contact, respectively.*

***Keywords*:** CZTSSe, superstrate, vacuum evaporation, thin film

## 1. Introduction

The thin film photovoltaic (PV) technologies have attracted a great deal of attention for past decade. The typical solar absorbers for thin-film PV, CdTe and Copper-Indium-Gallium-Sulfide (CIGS), have already achieved a lab-scaled cell efficiency of 22.1% [1] and 22.6% [2], respectively. The progress of this technology indicates great market share, but the great usage of highly-toxic Cd and limited In and Ga will make difficulties in real-world manufacturing. Thus, Copper-Zinc-Tin-Sulfide/Selenide (CZTSSe), an earth-abundant, non-toxic absorber with similar crystal and optical characteristics of CIGS, becomes another promising candidate material for thin-film PV. In addition, CZTSSe has an outstanding optical property: an adjustable direct bandgap within the region of 1.0-1.5 eV [3] and an absorption coefficient of $10^4$ $cm^{-1}$ [4] across the visible light spectrum.

CZTS/Se system was first developed by Ito *et al.* [5] and its photoelectric potential was also investigated. Various vacuum and non-vacuum deposition methods for CZTSSe have been developed since then: sputtering [6-7], evaporation [8-9], hot-injection [10], spin-coating [11], doctor-blading [12], electro-deposition [13-14] and powder metallurgy method [15]. Most devices are fabricated with substrate-configured cell structure similar to CIGS system and Mo is widely used as the back contact. The world record efficiency of CZTS/Se cell has already achieved 12.6% efficiency [16], but the large Sn loss during annealing process and the formation of $MoS_2$ between back contact and absorber layer still

ISSN 1512-1461

affects the performance of CZTSSe cells [17]. Thus, superstrate configuration is taken into consideration for CZTSSe cell fabrication to avoid those drawbacks. A CZTS superstrate cell with 0.36% efficiency was first fabricated by C. Shi *et al.* [18] by vacuum approach and this is by far the only record of vacuum-based CZTS superstrate cell. On the other hand, various non-vacuum based methods have been developed later. Detailed information of these technologies is summarized in Table 1. These works bring one step further for making high-efficient CZTS/Se superstrate solar cells, but the wide application of organic or toxic solvents in those non-vacuum methods might bring unwanted components into the absorber layer and may not suitable for the manufacturing of solar cell modules.

Table 1: Progress of superstrate-configured CZTS/Se solar cells by non-vacuum methods.

| **Device Structure** | **Fabrication Method** | **η (%)** | **$V_{oc}$ (mV)** | **$J_{sc}$ (mA/cm$^2$)** | **FF (%)** | **Ref.** |
|---|---|---|---|---|---|---|
| Carbon/CZTS/$In_2S_3$/$TiO_2$NP/FTO | Screen printing | 0.60 | 250 | 8.76 | 27.0 | [19] |
| Graphite/CZTS/CdS/FTO | Spray pyrolysis | 0.15 | 175 | 0.46 | 24.5 | [20] |
| Carbon/CZTS/$TiO_2$NP/$TiO_2$NP/TCO | Spray deposition | 0.51 | 564 | 2.85 | 43.0 | [21] |
| Au/CZTSSe/CdS/TiO2/ITO | Spin coating | 1.10 | 363 | 6.83 | 44.7 | [22] |
| Au/CZTS/CdS/ZnO NR/ITO | Spin coating | 1.20 | 679 | 4.10 | 43.8 | [23] |
| Au/CZTSe/CdS/ZnO NR/ITO | Spin coating | 2.44 | 443 | 13.72 | 41.1 | [24] |

This work includes the fabrication and characterization of vacuum-based CZTSSe solar cell with two different configurations: the best superstrate-configured cell shows an efficiency of 1.5% whereas the substrate-configured cell obtains a slightly higher efficiency of 2.2% and 2.0% with the ZnO layer inserted between CdS and ITO. It should be notified that our 1.5% efficiency is by far the best of vacuum-based superstrate-configured CZTSSe cell efficiency. Our cell also shows great progress in short circuit current density ($J_{sc}$). The structural and optical properties of the CZTSSe powder and thin film are also discussed.

## 2. Experimental Details

2.1 CZTSSe synthesis:

Our CZTSSe powder is synthesized by the following method. An aqueous solution of 0.134 M copper (II) sulfate ($CuSO_4 \cdot 5H_2O$), 0.067 M zinc nitrate ($Zn(NO_3)_2 \cdot 6H_2O$) and 0.067 M tin (IV) chloride ($SnCl_4 \cdot 5H_2O$, 98%) is made by dissolving these metals in 150 ml of water. 0.8 M thiourea ($CH_2SNH_2$) and 0.067 M selenium (IV) oxide ($SeO_2$) are added to the mixture afterwards. The mixture is sonicated for another 15 min and transferred into the autoclave. A preheating step is applied to increase the internal pressure to 15 psi. Then, the hydrothermal reaction lasts for 24 h. After the system is naturally cooled down, the black precipitate is filtered and washed with DI water and ethanol. After drying in argon under 110 $^oC$ for 1 h, the powder is sulfurized in argon under 550 $^oC$ for 1 h to prevent the sulfur loss during the reaction and assist the formation of CZTSSe phase.

ISSN 1512-1461

2.2 CZTSSe cell fabrication:

The superstrate CZTSSe cell is fabricated on a fluorine-doped $SnO_2$ coated glass substrate. The ZnO layer is deposited on the $SnO_2$layer by magnetron sputtering system. The CdS layer is fabricated by the CBD method [25]. A typical CdS deposition starts with $Cd(NO_3)_2$•$4H_2O$ (107 mg), $NH_4NO_3$ (255 mg), $CS(NH_2)_2$ (190.3 mg) and $NH_3$•$H_2O$ (3 ml). The overall 18-min deposition is processed at 80 ºC water bath heating while both solution and water bath are stirred under 600 rpm. The CBD step is processed twice to acquire adequate CdS film thickness. The as-deposited CdS layer is immediately rinsed with DI water and dried in a vacuum desiccator. The CdS layer is then annealed at 300 ºC for 1 h in Ar atmosphere. The CZTSSe layer is vacuum thermal-evaporated from our CZTSSe powder. The deposition current is gradually increased to 3 A. The deposition lasts for 10 min. After deposition, the absorber layer is sulfurized in argon at 280 ºC for 1 h. Patterned gold electrodes are deposited on CZTSSe layer by vacuum thermal evaporation to finish the device. An active area of 0.0225 $cm^2$ is divided by mechanical scribing. The substrate-configured CZTSSe solar cell starts with a Mo-coated soda-lime glass (SLG) substrate. The CZTSSe layer is deposited on Mo/SLG by the same vacuum evaporation method, followed by a post-sulfurization at 550 ºC in argon atmosphere. The sulfurization lasts for 1 h. The CdS window layer is deposited by the same method as shown above and the device is finally topped with the ITO electrode, which has a thickness of 300 nm. Some substrate-configured cells also have a sputtered ZnO layer before the deposition of ITO.

2.3 Characterization:

The crystal structure of CZTSSe is characterized with an X-ray diffractometry (PANalytical X'Pert Pro MPD) with Cu Kα radiation. Raman spectroscopy of CZTSSe is collected by a Jobin Yvon Horiba Confocal Raman Spectrometer. The surface morphologies of both CZTSSe and CdS film are examined by scanning electron microscope (SEM, Hitachi S-4800). CZTSSe film absorption spectrum is measured by using a double beam UV/Visible spectrometer (UV-1650 PC Shimadzu). The solar cell efficiency is characterized by a solar simulator with standard AM 1.5G (1 sun) irradiation.

**3. Results and Analysis**

Figure 1 and 2 show the XRD pattern of both as-synthesized CZTSSe powder and thin film. A clear kesterite phase could be identified from Figure 1 with peaks located at 28.4º, 32.9º, 47.3º, 56.1º, and 58.8º. These peaks, according to JCPDS 00-026-0575, could be assorted to planes (112), (200), (220), (312) and (224), respectively [26]**.** The peaks for (112), (220) and (312) are also the most dominant peaks in this XRD spectrum, indicating the kesterite phase has a much better crystal growth and serves as the most dominant phase in the compound. No peak for any binary or ternary phases could be observed, indicating the formation of phase-pure kesterite CZTSSe.

The peaks located at 26.8º, 30.9º and 47.6º observed from Figure 2 could be attributed to the planes (100), (021) and (400) of wurtzite CZTS and they match well with previous experimental and simulated results [27, 28]. The other two major peaks located at 28.6º and 33.0º demonstrate the existence of kesterite CZTSSe phase in our thin film. Neither of wurtzite and kesterite CZTSSe could be able to occupy the dominant position by comparing their peak intensities. The low-temperature annealing process could be the reason of such CZTSSe recrystallization results since the wurtzite phase could be converted into kesterite CZTS with 550 ºC annealing with the presence of sulfur **[29].**

ISSN 1512-1461

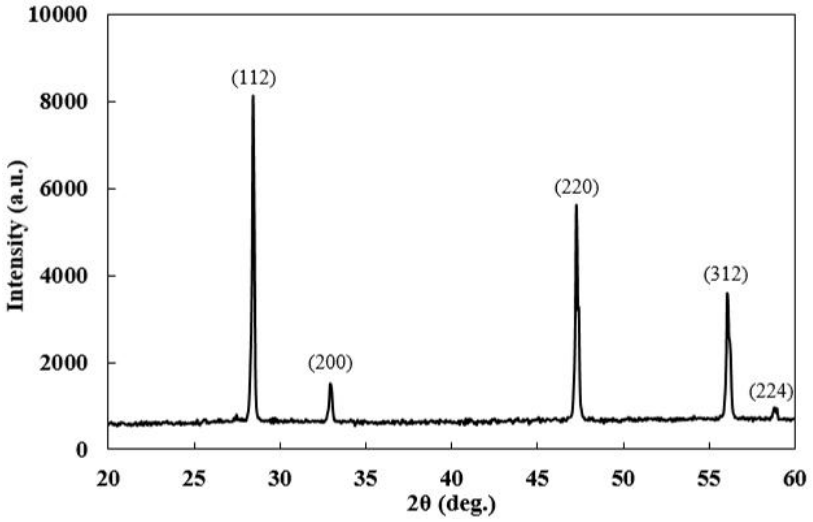


Figure 1: XRD spectrum of sulfurized CZTSSe powder source.

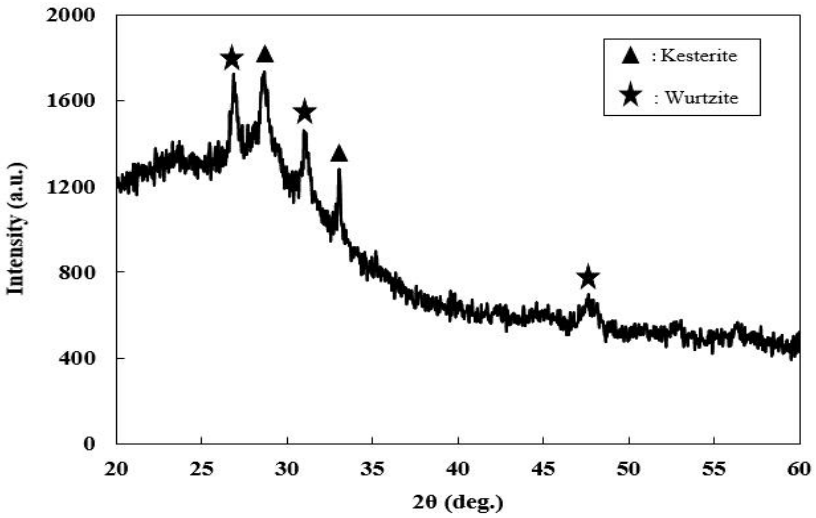


Figure 2: XRD spectrum of sulfurized CZTSSe thin film.

The Raman spectrum of the annealed CZTSSe thin film is displayed in Figure 3 as the verification of the formation of kesterite CZTSSe phase. Our result showed a strong peak at 325 $cm^{-1}$, and a wide secondary peak around 219 $cm^{-1}$, which has some shift compared with the typical Raman peaks for CZTS and CZTSe: the Raman peaks for $A_1$ pure anion mode CZTS and CZTSe were 339 $cm^{-1}$ and 196 $cm^{-1}$, respectively [30]. This shift could result in the appearance of wurtzite CZTS together with the existence of Se, which has been already demonstrated in another earlier research [31]. No peaks of several common binary or ternary phases, such as ZnS appeared at 348 $cm^{-1}$ or 356 $cm^{-1}$, $Cu_2SnS_3$ at 336 $cm^{-1}$ or 351 $cm^{-1}$ [32] could be observed from Figure 3. Our Raman spectra, therefore, demonstrates the formation of the CZTSSe layer with no binary and ternary phases.

ISSN 1512-1461

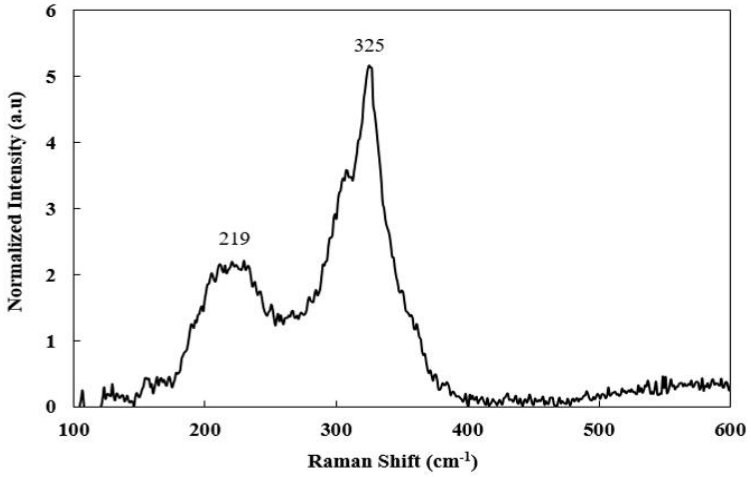


Figure 3: Raman spectra of sulfurized CZTSSe thin film.

The SEM image in Figure 4 (a) indicates a void-free surface morphology of the CZTSSe film. The shiny part at the left bottom is due to the excess sulfur during the sulfurization process. All grains are closely packed, and the wurtzite phase does not affect film surface morphology. The average grain size could be roughly estimated to be 100-200 nm. The surface morphology of annealed CdS film before the deposition of CZTSSe is shown in Figure 4 (b). It can be seen that both CdS and CZTSSe share the similar range of grain sizes, but some tiny CdS nano-particles increases the surface roughness of CdS layer. Thus, the CZTSSe/CdS interface could have a complicated structure, which may limit the performance of the solar cell.

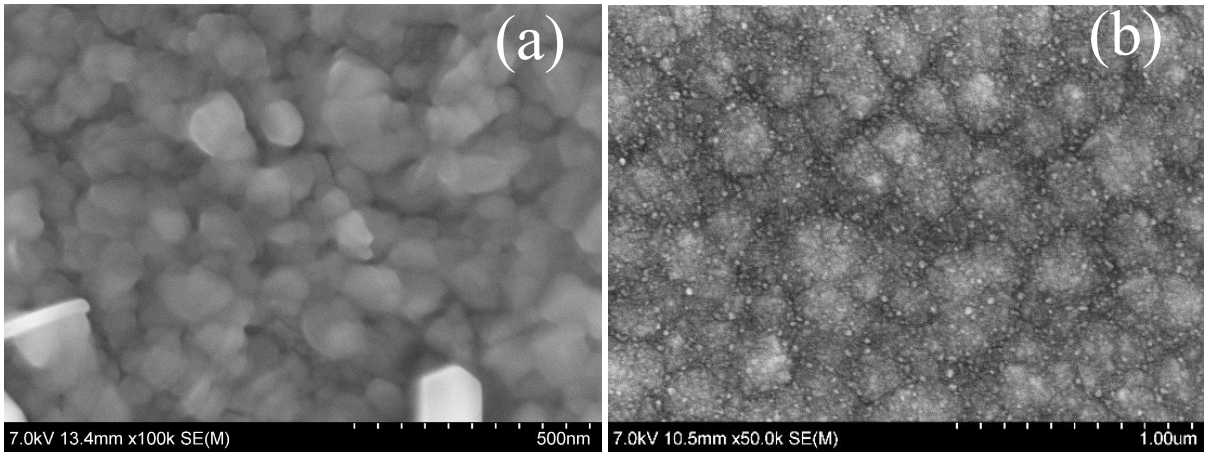


Figure 4: SEM image of the surface of (a) sulfurized CZTSSe film and (b) annealed CdS film.

The optical absorption coefficient spectrum in the visible and near-infrared area is shown in Figure 5 (a). It could be observed from this spectrum that the absorption coefficient is maintained above $10^4$ $cm^{-1}$ during the whole measurement. The absorption coefficient keeps increasing rapidly all over the visible light spectrum, which indicates the great visible light absorption potential of this CZTSSe film.

The bandgap analysis of CZTSSe absorption layer is shown in Figure 5 (b). The plot uses Tauc's model to estimate the bandgap of the sulfurized CZTSSe film. Figure 5 (b) shows that this sulfurized CZTSSe film has a bandgap of 1.53 eV. This bandgap value matches well with other band gap results

ISSN 1512-1461

of both kesterite [33, 34] and wurtzite [35, 36] CZTS with a band gap region of 1.4-1.6 eV [26]. This plot also demonstrates that our CZTSSe thin film has a direct band gap structure by using $(\alpha h\nu)^2$ versus photon energy. It could be further observed that by applying this bandgap result back into Figure 5 (a), the absorption coefficient would always be higher than $2x10^4$ $cm^{-1}$ in the 'working region' of CZTSSe, which again demonstrates the great sunlight absorption potential of our CZTSSe film.

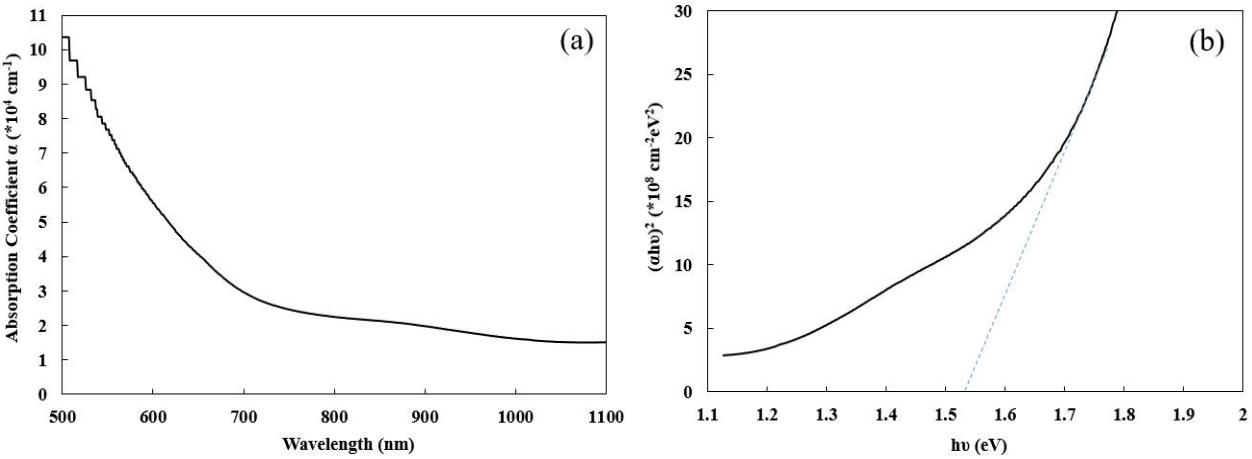


Figure 5: (a) The UV-Vis spectrum of absorption coefficient versus wavelength and (b) Band gap analysis of the sulfurized CZTSSe thin film.

Superstrate-configured CZTSSe solar cell is fabricated and characterized with an active area of 0.0225 $cm^2$. The current density-voltage (J-V) characterization of our best cell is displayed in Figure 6. This J-V curve shows a $J_{sc}$ of 15.6 $mA/cm^2$, a $V_{oc}$ of 221 mV, an efficiency (η) of 1.5% and a fill factor (FF) of 43% for our best cell with Au back contact. The test is finished under standard AM 1.5G illumination. Our best device, compared with the previous vacuum-based result, achieves a significant increase in $J_{sc}$. The relatively low $V_{oc}$ may be due to the absence of suitable transparent high-resistive blocking layer which could reduce the carrier recombination.

An estimation of series and shunt resistance of both cells under illumination is calculated by finding the inverse slope dV/dJ against voltage near $J_{sc}$ and $V_{oc}$. The Au-topped CZTSSe cell shows a series resistance ($R_s$) of 347.6 $\Omega.cm^2$ and a shunt resistance ($R_{sh}$) of 1557.9 $\Omega.cm^2$. This series resistance is too high that leads to a relatively lower $J_{sc}$. The complicated surface morphologies observed for both CZTSSe and CdS surfaces shown in Figure 4 (a) also brings disadvantages: some excess sulfur occupies the CZTSSe surface. These sulfur particles may become a barrier between CZTSSe and metal contact, blocking the carrier collection of the device and could be one source of the high series resistance of the solar cell. The rough surface of CdS layer would let some small CZTSSe grains mix with CdS in the interface area. Such phase mixing across the CZTSSe/CdS interface area has both advantages and drawbacks: the advantage is that this kind of phase mixing would passivate the recombination within the interface region and therefore, increase the excited electron transportation [35]. The drawbacks, however, is due to the non-planer surface structure of CdS as shown in Figure 4 (b). The CZTSSe layer, therefore, may not have a perfect surface coverage across the junction interface, leaving some unwanted shunting paths and low shunt resistance. Those nano-scaled pinholes could be another factor that reduced our $V_{oc}$. The small grain size generated by low-temperature sulfurization would also create extra recombination centers across the whole p-type layer, decreasing the carrier diffusion length and reducing the overall $V_{oc}$ and $J_{sc}$.

ISSN 1512-1461

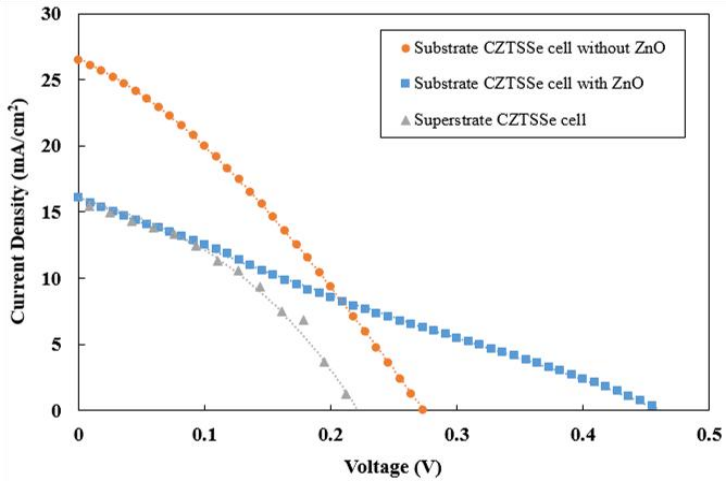


Figure 6: J-V characteristics of the best superstrate and substrate CZTSSe solar cell devices with/without ZnO layer.

The superstrate-configured CZTSSe cell structure also has its natural limitations. Since high-temperature heating could drastically amplify the negative effect of Cd diffusion, in which a large amount of CZTSSe layer may become intrinsic or n-type conductivity due to Cd doping. The stoichiometric ratio of CZTSSe would also be affected, and the corresponding resistivity and other electrical and optical properties might be changed. Other research regards the elemental composition across the CZTSSe device found the Zn and Se tends to shift to the CdS side while Cd could be found deep inside the CZTSSe or even close to the back contact [38-40]. Those deep-buried Cd atoms also show some potential correlations with pinholes inside CZTSSe [39]. The negative effect of Cd diffusion on the performance of CZTSSe solar cell has been already observed in the substrate-configured CZTSSe cells, where the solar cell parameters would decrease, and the rectifying behavior of J-V characteristics would be reduced with extended CdS deposition time [41]. There is still not much detailed discussion on the effect of Cd diffusion in the fabrication of superstrate CZTSSe cell, but since the CZTSSe re-crystallization is processed on CdS, the Cd diffusion into CZTSSe crystal could hardly be avoided. A previous study showed that a charge-neutral ($Cd_{Cu}$ + $V_{Cu}$) vacancy pair together with few n-type $Cd_{Cu}$ and neutral $Cd_{Zn}$ would be formed during the CBD process [42]. Similar behavior could be then expected during the formation of CZTSSe on the surface of CdS. Thus, better optimization of CZTSSe re-crystallization conditions under low temperature is suggested for developing better superstrate CZTSSe solar cells. The co-existence of wurtzite and kesterite CZTSSe might also have an unknown effect on the device performance and need more work to understand.

Two substrate-configured CZTSSe cells, with or without the high-resistive ZnO layer, are fabricated and characterized. The results are also displayed in Figure 6. The cell without ZnO shows a higher $J_{sc}$ of 26.5 mA/cm$^2$, an increased $V_{oc}$ of 273 mV, a better FF of 30% and a higher efficiency of 2.2%. The device with ZnO has a relatively lower $J_{sc}$ of 16.3 mA/cm$^2$, a significantly high $V_{oc}$ of 463 mV, a decreased FF of 27% and a slightly lower efficiency of 2.0%. Both cells show a clear increase of $V_{oc}$, which could be due to the advantage of substrate-configuration where less Cd would disturb the absorption layer. The existence of ZnO also offers a great enhancement of $V_{oc}$ because ZnO serves as a blocking layer between CdS and ITO. This blocking layer could enhance the device shunting and reduce the carrier combination at the CdS/ITO interface. The clear decrease of $J_{sc}$ of the ZnO-equipped reference cell, however, may also be due to the high resistivity of ZnO which blocks carriers from

ISSN 1512-1461

being collected by the front contact. This comparison indicates our ZnO requires better thickness control.

Both substrate-configured cells show a higher efficiency than our superstrate solar cells, which could be due to a higher sulfurization temperature of CZTSSe layer. The CZTSSe grains could be able to have a better growth in this case, and the density of grain boundaries are therefore, decreased, leaving fewer traps for charge transportation and fewer chances for carrier recombination. A relatively low FF could be described as the formation of low-quality p-n junctions, which may be related to the non-ideal carrier transportation in the CdS layer. The excess Cd diffusion during the deposition of CdS could also reduce the formation of high-quality p-n junction, which happens on our superstrate CZTSSe devices. The improved quality of CZTSSe layer before the joint of CdS, however, leads to a higher device efficiency due to a less Cd diffusion into the absorption layer compared with the superstrate-configured CZTSSe cell, where CZTSSe re-crystallization is processed with the existence of CdS.

## 4. Conclusion

Superstrate solar cell was fabricated using vacuum coated CZTSSe. The CZTSSe powder was synthesized by an aqueous hydrothermal method. A low-temperature sulfurization step is applied for the CZTSSe layer, and its effects are studied by XRD, Raman, and SEM. The results show the formation of both wurtzite and kesterite CZTSSe structures together with void-free and close-packed small grains. A high absorption coefficient of this CZTSSe thin film is estimated and the corresponding direct bandgap energy is estimated to be 1.53 eV, which is close to the bandgap of both phase-pure wurtzite and kesterite CZTS. A record vacuum-based superstrate-configured solar cell efficiency of 1.5% is obtained under standard sunlight. The $J_{sc}$ of our best cell is boosted compared with the previous vacuum-based device, but the $V_{oc}$ and FF are still relatively low. The co-existence of wurtzite and kesterite phases and the low sulfurization temperature may be the reasons for lower $V_{oc}$ and FF. Two substrate-configured CZTSSe solar cells with and without ZnO blocking layer was also fabricated and tested. Both of them showed higher efficiency (2.0% and 2.2%, respectively) and higher $V_{oc}$. These higher efficiencies from the substrate-configured CZTSSe cells could be due to a better growth of CZTSSe and relatively lower Cd diffusion during the fabrication of solar cell. The low FF and low $J_{sc}$ in the ZnO-equipped cell, however, still indicated that better optimization should be done on the growth of CdS and ZnO layers to improve the quality of the junction characteristics. More work is suggested for the demonstration and elevation of superstrate CZTSSe solar cell efficiency.

## References

1. J. Ramanujam and U. P. Singh, Energy & Environmental Science, (2017) , 10, 1306.
2. I. M. Dharmadasa, O. K. Echendu, and F. Fauzi, J Mater Sci: Mater Electron (2017), 28, 2343.
3. F. J. Fan, L. Wu, M. Gong, G. Liu, Y. Wang, S. Yu, S. Chen, L. Wang, and X. Gong, ACS Nano (2013), 7, 1454.
4. D. B. Mitzi, O. Gunawan, T. K. Todorov, K. Wang, and S. Guha, Sol. Energ. Mat. Sol. Cells (2011), 95, 1421.
5. K. Ito and T. Nakazawa, Jpn. J. Appl. Phys. (1988) ,27,2094.
6. R. Lechner, S. Jost, J. Palm, M. Gowtham, F. Sorin, B. Louis, H. Yoo, R. A. Wibowo, and R. Hock, Thin solid films, (2013), 535, 5.
7. J. Márquez, M. Neuschitzer, M. Dimitrievska, R. Gunder, S. Haass, M. Werner, Y. E. Romanyuk, S. Schorr, N. M. Pearsall, and I. Forbes, Solar Energy Materials and Solar Cells, 144 (2016) 579.
8. H. Katagiri, N. Sasaguchi, S. Hando, S. Hoshino, J. Ohashi, and T. Yokota, Solar Energy Materials and Solar Cells, (1997), 49 407.

ISSN 1512-1461


9. Y. S. Lee, T. Gershon, O. Gunawan, T. K. Todorov, T. Gokmen, Y. Virgus, and S. Guha, Advanced Energy Materials, 5 (2015) 1401372.
10. N. Mirbagheri, S. Engberg, A. Crovetto, S. B. Simonsen, O. Hansen, Y. M. Lam, and J. Schou, Nanotechnology 27 (2016) 185603.
11. R. Liu, M. Tan, X. Zhang, J. Chen, S. Song, and W. Zhang, Journal of Alloys and Compounds 655 (2016) 124.
12. C. K. Miskin, W. C. Yang, C. J. Hages, N. J. Carter, C. S. Joglekar, E. A. Stach, and R. Agrawal, Progress in Photovoltaics: Research and Applications, 23 (2015) 654.
13. J. J. Scragg, P. J. Dale, L. M. Peter, G. Zoppi, and I. Forbes, Physica Status Solidi B, 245 (2008) 1772.
14. L. Vauche, L. Risch, Y. Sánchez, M. Dimitrievska, M. Pasquinelli, T. G. de Monsabert, P. P. Grand, S. J. Ferrer, and E. Saucedo, Progress in Photovoltaics: Research and Applications, 24 (2016) 38.
15. Z. Shi, D. Attygalle, and A. H. Jayatissa, Journal of Materials Science: Materials in Electronics 28 (2017) 2290.
16. W. Wang, M. T. Winkler, O. Gunawan, T. Gokmen, T. K. Todorov, Y. Zhu, and D. B. Mitzi, Advanced Energy Materials, 4 (2014) 1301465.
17. J. J. Scragg, T. Kubart, J. T. Wätjen, T. Ericson, M. K.Linnarsson, and C. Platzer-Björkman, Chemistry of Materials 25 (2013) 3162.
18. C. Shi, G. Shi, Z. Chen, P. Yang, and M. Yao, Materials Letters 73 (2012) 89.
19. Q. M. Chen, S. Y. Cheng, S. L. Zhuang, and X. M. Dou, Thin Solid Films 520 (2012) 6256.
20. M. Patel, I. Mukhopadhyay, and A. Ray, Journal of Physics D: Applied Physics 45 (2012) 445103.
21. M. Kurokawa, K. Tanaka, K. Moriya, and H. Uchiki, 2012 Japanese Journal of Applied Physics 51 (2012) 10NC33.
22. C. L. Wang and A. Manthiram, ACS Sustainable Chemistry and Engineering 2 (2014) 561.
23. D. Lee and K. Yong, Nanotechnology 25 (2014) 065401.
24. Y. Zhang, Y. Sun, H. Wang, and H. Yan, Physica Status Solidi A 213 (2016) 1324.
25. M. Gautam, Z. Shi, and A.H. Jayatissa, Solar Energy Mater. Solar Cells 163 (2017) 1.
26. Z. Shi and A.H. Jayatissa, Prog. Nat. Sci. Mater. Int. 27 (2017) 550.
27. E. Ha, L. Y. S. Lee, J. Wang, F. Li, K. Y. Wong, and S. C. E. Tsang, Advanced Materials, 26 (2014) 3496.
28. H. Jiang, P. Dai, Z. Feng, W. Fan, and J. Zhan, Journal of Materials Chemistry, 22 (2012) 7502.
29. Z. X. Chang, W. H. Zhou, D. X. Kou, Z. J. Zhou, and S. X. Wu, Chemical Communications, 50 (2014) 12726.
30. D. Park, D. Nam, S. Jung, S. An, J. Gwak, K. Yoon, J. H. Yun, and H. Cheong, Thin Solid Films, 519 (2011) 7386.
31. M. Grossberg, J. Krustok, J. Raudoja, K. Timmo, M. Altosaar, and T. Raadik, Thin Solid Films, 519 (2011) 7403.
32. J. He, L. Sun, S. Chen, Y. Chen, P. Yang, and J. Chu, J. Alloys and Compounds, 15 (2012) 129.
33. Y. Cao, M. S. Denny Jr., J. V. Caspar, W. E. Farneth, Q. Guo, A. S. Lonkin, L. K. Johnson, M. Lu, I. Malajovich, D. Radu, H. D. Rosenfeld, K. R. Choudhury, and W. Wu, Journal of the American Chemistry Society, 134 (2012) 15644.
34. X. Zhang, G. Guo, C. Ji, K. Huang, C. Zha, Y. Wang, L. Shen, A. Gupta, and N. Bao, Scientific Reports, 4 (2014) 5086.
35. X. Lu, Z. Zhuang, Q. Peng, and Y. Li, Chemical Communications, 47 (2011) 3141.
36. A. Singh, H. Geaney, F. Laffir, and K. M. Ryan, Journal of the American Chemistry Society, 134 (2012) 2910.

ISSN 1512-1461

37. M. Werner, D. Keller, S. G. Haass, C. Gretener, B. Bissig et al., ACS Applied Materials Interfaces, 7 (2015) 12141.
38. T. Kato, H. Hiroi, N. Sakai, and H. Sugimoto, 28th European Photovoltaic Solar Energy Conference and Exhibition, (2013), 2125.
39. J. W. Cho, A. Ismail, S. J. Park, W. Kim, S. Yoon, and B. K. Min, ACS Applied Materials and Interfaces, 5 (2013), 4162.
40. T. Gershon, C. Hamann, M. Hopstaken, Y. S. Lee, B. Shin, and R. Haight, Advanced Energy Materials, 5 (2015), 1500922.
41. K. Tanaka, M. Oonuki, N. Moritake, and H. Uchiki, Solar Energy Materials and Solar Cells, 93 (2009) 583.
42. T. Maeda, S. Nakamura, and T. Wada, Japanese Journal of Applied Physics, 51 (2012) 10NC11.

Article received: 2020-03-08